Giant longitudinal spin Hall effect for elliptically polarized light under surface plasmon resonance

Ze Chen[1] **, Weiming Zhen**[2,*] **, Hua Xu**[1]**, Guoce Zhuang**[1]**, Zhihai Zhang**[1]**, Hu Zhang**[3]**, Xiaoguang Zhang**[3] **and Yang Meng**[4,*]

[1] School of Physics and Electronic Engineering, Yancheng Teachers University, Yancheng, People's Republic of China
[2] School of Physics, Nanjing University, Nanjing, People's Republic of China
[3] State Key Laboratory of Information Photonics and Optical Communications, Beijing University of Posts and Telecommunications, Beijing, People's Republic of China
[4] Institute of Mechanics, Chinese Academy of Sciences, Beijing, People's Republic of China

E-mail: wmzhen@smail.nju.edu.cn and mengyang@imech.ac.cn

Abstract

We propose a novel and simple method for obtaining the giant longitudinal spin Hall effect (SHE) of the reflected light beam when the elliptically polarized light (instead of the linearly polarized light) at the telecommunication wavelength is obliquely incident on a prism–sodium interface excited by surface plasmon resonance. By introducing the spatially averaged Stokes parameter $\bar{S}_3$ for a non-uniformly polarized reflected light field, understanding the generation mechanism of the giant longitudinal SHE from a new perspective is realized. The giant longitudinal SHE under the elliptically polarized light reaches 60.28 μm by the optimal parameter setup, and the spin splitting direction of the SHE can be switched by adjusting the amplitude ratio angle and phase difference of the incident elliptically polarized light. These findings open the way for the precise measurement of the ellipticity of the elliptically polarized light and the design of novel fiber-optic devices.

Keywords: spin Hall effect of light, elliptically polarized light, surface plasmon resonance

(Some figures may appear in colour only in the online journal)

1. Introduction

When a spatial bounded light beam with horizontal or vertical polarization impinges onto a plane interface between two media with different refractive indices, reflected and transmitted beams, a transverse symmetric spin splitting (TSSS) in the direction perpendicular to the plane of incidence occurs [1, 2]. From the perspective of light–matter interaction, the TSSS of light originates from the spin angular momentum to extrinsic orbital angular momentum conversion [3]. It is also known as the spin Hall effect (SHE) of light [1, 2, 4], which has attracted widespread attention owing to its potential application in spatial differential operation [5], edge imaging [6], and probing topological quantum phase transitions [7]. Interestingly, an anomalous photonic SHE caused by significant destructive interferences between normal and abnormal modes has recently been reported [8–10]. Besides, there also exists a longitudinal symmetric spin splitting (LSSS) of light in the direction parallel to the plane of incidence, which is equally important for enriching the concept of spin photonics [11]. However, the TSSS or LSSS is generally so small compared to the wavelength that it is difficult to directly observe in the experiment. There have been several methods to amplify

* Authors to whom any correspondence should be addressed.

the TSSS or LSSS among the weak amplification technology (including isotropic and anisotropic interfaces) [2, 12–14], near Brewster incidence [15], surface plasmon resonance (SPR) [16, 17], and so on [18–21]. It is worth noting that all the incident light chosen to achieve larger TSSS or LSSS is linearly polarized. Since the angular longitudinal SHE of linearly polarized light is relatively large, the transverse or longitudinal SHE can be enhanced by intrinsic orbital angular momentum (IOAM) [14] and transmission distance of the light beam [22], respectively.

Interestingly, the properties of the elliptically polarized light have attracted the attention of many researchers due to potential applications in high-harmonic generation enhancement [23], measurement of complex optical susceptibility [24], photoelectron holography, and forward scattering [25]. However, the precise measurement of ellipticity is a key issue that affects the application prospects of elliptically polarized light [26]. Achieving giant TSSS or LSSS based on incident elliptically polarized light is expected to open up a new way to solve the precision measurement of the ellipticity for the elliptically polarized light. A method to quantitatively identify TSSS and transverse asymmetric spin splitting of arbitrarily polarized light reflected under weak spin–orbit coupling conditions have been proposed by introducing a spin splitting factor [27]. Nevertheless, there are still some problems that need to be solved urgently about the TSSS or LSSS of the elliptically polarized light. For example, its size is too small to be directly observed, only occurs in the transverse direction, and the spin-independent shift is not very small relative to the TSSS or LSSS. We put forward a new and important question now: can the spatial TSSS or LSSS of the reflected light be amplified directly without the aid of IOAM and transmission distance?

In this work, we rigorously derive the analytical expression of the spatial longitudinal spin splitting for arbitrarily polarized light reflected through a plane interface based on the operator formalism. We reveal the generation mechanism of the LSSS in reflection of arbitrary elliptically polarized light from two perspectives: the analysis of asymmetric spin splitting factor and the spatially averaged Stokes parameter $\bar{S}_3$, which provides a novel and simple way to generate the giant longitudinal SHE when an elliptically polarized light at the telecommunication wavelength is reflected on a prism–sodium interface excited by SPR. It is worth emphasizing that this giant longitudinal SHE of elliptically polarized light is realized for the first time to our knowledge.

2. Theoretical model for the LSSS of arbitrarily polarized light by the SPR

A novel Kretschmann configuration with a sodium thin film coated on a glass prism is adopted, as shown in figure 1. In general, the Kretschmann configuration for enhancement of photonic SHE, silver and gold are chosen as plasmonic materials owing to their relatively low loss, but their optical loss is still not commercially acceptable and has been the primary limiting factor for the widespread applications of the
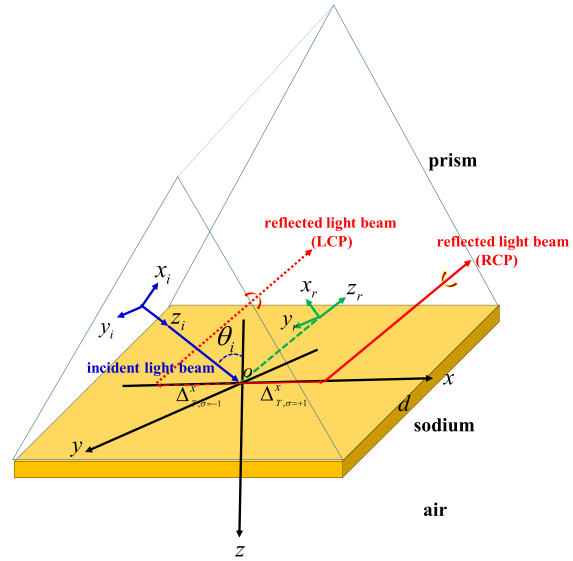
Figure 1. Schematic illustration of the longitudinal SHE of an arbitrarily polarized light beam in the Kretschmann configuration, $\Delta_{T,\sigma=+1}^{x}$ and $\Delta_{T,\sigma=-1}^{x}$ represent the LSSSs for the left- and right-handed circularly polarized components of the reflected beam on the interface, respectively, where $\Delta_{T,\sigma}^{x} = \Delta_{T,\sigma}/\cos\theta_r$ $\theta_r = \arccos(\hat{\mathbf{z}}_r \cdot \hat{\mathbf{z}})$.

SPR [28, 29]. Sodium, which is also regarded as an ideal plasmonic material, has been predicted for many years. However, manufacturing sodium-based structures by conventional metal deposition techniques are still full of great challenges due to its high chemical reactivity. Fortunately, Wang *et al* has recently demonstrated a method of fabricating high-quality sodium films [30]. It is shown clearly that its superior performance at telecommunications wavelengths is very obvious by comprehensive comparison with the previously reported devices based on noble metals.

In this model, the relative permittivities of glass, sodium, and air are represented by ε_1, $\varepsilon_2(\omega)$ (ω being the angular frequency of the incident light beam), and ε_3, respectively. Now, a monochromatic polarized light beam of wavelength λ_0 and the waist w_0 propagates along the central wave vector $\mathbf{k}_c^i$ impinging upon the glass prism–sodium interface ($z = 0$), where $|\mathbf{k}_c^i| = 2\pi\sqrt{\varepsilon_1}/\lambda = \sqrt{\varepsilon_1}\omega/c$ (c being the velocity of the incident light beam in vacuum). The geometry of beam reflection is also depicted in figure 1, and $\theta_i = \arccos(\hat{\mathbf{z}}_i \cdot \hat{\mathbf{z}})$ is the incident angle. The incident and reflected beams are denoted by the superscripts $a = i, r$, respectively, and the basics of the central Cartesian coordinate frame for ath beam is represented by $\hat{\mathbf{x}}_a$, $\hat{\mathbf{y}}_a$ and $\hat{\mathbf{z}}_a$, respectively. The momentum representation of the electric field for the incident light beam is expressed as:

$$\left|\tilde{E}^i\right\rangle = \frac{w_0^2}{2\pi}\sum_{\rho=P}^{S}a_{i,\rho}\left|\tilde{e}_{i,\rho}\right\rangle\exp\left[-\frac{(k_x^i)^2+(k_y^i)^2}{4w_0^{-2}}\right], \rho\in\{P,S\},$$

$$(1)$$

where $k_x^i = \mathbf{k}^i \cdot \hat{\mathbf{x}}_i$, $k_y^i = \mathbf{k}^i \cdot \hat{\mathbf{y}}_i$ with $|\mathbf{k}^i| = |\mathbf{k}_c^i| = k^i$, $|\tilde{e}_{i,P}\rangle = (1,0)_{\text{LPB}}^{\dagger}$ and $|\tilde{e}_{i,S}\rangle = (0,1)_{\text{LPB}}^{\dagger}$, the superscript $\dagger$ and subscript

LPB are conjugate transpose operator and two-dimensional row vector in a linear polarization basis respectively. $a_P = \cos\alpha$, $a_S = \sin\alpha\exp(i\Delta\phi)$, where α denotes the amplitude ratio angle, and $\Delta\phi$ is the phase difference between P and S components of the electric field of the incident light beam.

In order to apply the Fresnel equation exactly to each plane wavelet, the polarization of the incident light field is transformed from the incident laboratory coordinate system to the local coordinate system, which can be expressed as

$$\left|\tilde{E}_{\mathrm{loc}}^{i}\right\rangle = \hat{\mathbf{R}}^{i}\left|\tilde{E}^{i}\right\rangle, \tag{2}$$

with $\hat{\mathbf{R}}^{i} = \begin{pmatrix} 1 & \frac{k_y^i}{k^i}\cot\theta_i \\ -\frac{k_y^i}{k^i}\cot\theta_i & 1 \end{pmatrix}$.

According to the Fresnel Equation, the momentum representation of the reflected optical field in the reflected local coordinate system can be given by

$$\left|\tilde{E}_{\mathrm{loc}}^{r}\right\rangle = \hat{F}^{r}\left|\tilde{E}_{\mathrm{loc}}^{i}\right\rangle, \tag{3}$$

where $\hat{F}^{r} = \begin{pmatrix} \tilde{r}_P & 0 \\ 0 & \tilde{r}_S \end{pmatrix}$, which is the reflection Fresnel matrix operator. In order to obtain the analytical solution of longitudinal spin splitting, it is necessary to make a first-order Taylor expansion of $\tilde{r}_p$ and $\tilde{r}_S$ at $k_x^i = 0$, $k_y^i = 0$ (i.e. the central incidence angle) [31]

$$\tilde{r}_P = \tilde{r}_P(k_x^i = 0, k_y^i = 0) + \frac{\partial\tilde{r}_P}{\partial(k_x^i/k^i)}\frac{k_x^i}{k^i}, \tag{3a}$$

$$\tilde{r}_S = \tilde{r}_S(k_x^i = 0, k_y^i = 0) + \frac{\partial\tilde{r}_S}{\partial(k_x^i/k^i)}\frac{k_x^i}{k^i}, \tag{3b}$$

where $\tilde{r}_P(k_x^i = 0, k_y^i = 0) = r_P$, $\tilde{r}_S(k_x^i = 0, k_y^i = 0) = r_S$, $\partial\tilde{r}_P/\partial(k_x^i/k^i) = \partial r_P/\partial\theta_i$, $\partial\tilde{r}_S/\partial(k_x^i/k^i) = \partial r_S/\partial\theta_i,$. Then, $\hat{\mathbf{F}}^{r}$ can be further expressed as

$$\hat{\mathbf{F}}^{r} = \begin{pmatrix} r_P + \frac{\partial r_P}{\partial\theta_i}\frac{k_x^i}{k^i} & 0 \\ 0 & r_S + \frac{\partial r_S}{\partial\theta_i}\frac{k_x^i}{k^i} \end{pmatrix}. \tag{3c}$$

For the Kretschmann configuration, the reflection coefficients can be written as [32]:

$$r_{P/S} = \frac{r_{P/S}^{12} + r_{P/S}^{23}e^{2ik_{z2}d}}{1 + r_{P/S}^{12}r_{P/S}^{23}e^{2ik_{z2}d}}, \tag{3d}$$

where $r_P^{12} = (\varepsilon_2 k_{z1} - \varepsilon_1 k_{z2})/(\varepsilon_2 k_{z1} + \varepsilon_1 k_{z2})$, $r_P^{23} = (\varepsilon_3 k_{z2} - \varepsilon_2 k_{z3})/(\varepsilon_3 k_{z2} + \varepsilon_2 k_{z3})$, $r_S^{12} = (k_{z1} - k_{z2})/(k_{z1} + k_{z2})$, $r_S^{23} = (k_{z2} - k_{z3})/(k_{z2} + k_{z3})$ with $k_{z1} = k^i\sqrt{\varepsilon_1}\cos\theta_i$, $k_{z2} = k^i\sqrt{\varepsilon_2 - \varepsilon_1\sin^2\theta_i}$, $k_{z3} = k^i\sqrt{\varepsilon_3 - \varepsilon_2\sin^2\theta_i}$ are the z components of the wave vectors of the incident light beam.

Considering the convenience of observing the reflected light field, a mirror-symmetry reflection operator with respect to the x_i-axis $\hat{M}^r$, which is introduced to transform the reflected light field from coordinate (k_x^i, k_y^i) to coordinate (k_x^i, k_y^r). The mirror-symmetry reflection operator satisfies the relation: $\hat{\mathbf{M}}^r\left|\tilde{E}(k_x^i, k_y^i)\right\rangle = \left|\tilde{E}(-k_x^i, k_y^r)\right\rangle$. Finally, using the transformation matrix of the reflection local coordinate system to

the reflection laboratory coordinate, the reflection light field momentum representation in the reflection laboratory coordinate system can be written as

$$\left|\tilde{E}^{r}\right\rangle = \left(\hat{\mathbf{R}}_{\theta_r\mapsto\pi-\theta_i}^{r}\right)^{\dagger}\left|\tilde{E}_{\mathrm{loc}}^{r}\right\rangle. \tag{4}$$

Through the above detailed description of the reflection process of the paraxial polarized light field, the whole reflection process experienced by the paraxial light field can be described by a scattering operator $\hat{S}^r$. The scattering operator $\hat{S}^r$ satisfies the following relationship: $\left|\tilde{E}^r(k_x^r, k_y^r)\right\rangle = \hat{S}^r\left|\tilde{E}^i(k_x^i, k_y^i)\right\rangle$, where $\hat{S}^r = (\hat{\mathbf{R}}^r)^{\dagger}\hat{\mathbf{M}}^r\otimes\hat{F}^r\hat{\mathbf{R}}^i$. Furthermore, from equations (1) to (4), it follows that

$$\left|\tilde{E}^{r}\right\rangle = \frac{w_0^2}{2\pi}\sum_{\rho=P}^{S}b_{r,\rho}\left|\tilde{e}_{r,\rho}\right\rangle\exp\left[-\frac{(k_x^r)^2 + (k_y^r)^2}{4w_0^{-2}}\right], \tag{5}$$

where $b_{r,\rho}$ is replaced by b_P^r for $\rho = P$ and b_S^r for $\rho = S$, respectively. The b_P^r and b_S^r can be given as

$$b_{r,P} = r_P a_P\left(1 - \frac{k_x^r}{k^i}\frac{\partial r_P}{r_P\partial\theta_i} + \frac{k_y^r}{k^i}\frac{r_P + r_S}{r_P}\frac{a_S\cot\theta_i}{a_P}\right), \tag{5a}$$

$$b_{r,S} = r_S a_S\left(1 - \frac{k_x^r}{k^i}\frac{\partial r_S}{r_S\partial\theta_i} - \frac{k_y^r}{k^i}\frac{r_P + r_S}{r_S}\frac{a_P}{a_S}\cot\theta_i\right). \tag{5b}$$

By using the relation: $\left|\tilde{e}_{r,P}\right\rangle = (\left|\tilde{e}_{r,+1}\right\rangle + \left|\tilde{e}_{r,-1}\right\rangle)/\sqrt{2}$, $\left|\tilde{e}_{r,S}\right\rangle = -i(\left|\tilde{e}_{r,+1}\right\rangle - \left|\tilde{e}_{r,-1}\right\rangle)/\sqrt{2}$, where $\left|\tilde{e}_{r,+1}\right\rangle = (1,0)_{\mathrm{CPB}}^{\dagger}$ and $\left|\tilde{e}_{r,-1}\right\rangle = (0,1)_{\mathrm{CPB}}^{\dagger}$, the sub-script CPB is a two-dimensional row vector on circular polarization basis. Then, from equation (5) it readily follows that

$$\left|\tilde{E}_{\sigma}^{r}\right\rangle = \frac{w_0^2 r_P a_P}{2\sqrt{2}\pi}\sum_{\sigma=+1}^{-1}c_{r,\sigma}\left|\tilde{e}_{r,\sigma}\right\rangle\exp\left[-\frac{(k_x^r)^2 + (k_y^r)^2}{4w_0^{-2}}\right], \tag{6}$$
$$\sigma\in\{+1, -1\},$$

where $c_{r,\sigma} = (1 - i\sigma b_2)(1 - ik_x^r X_{r,\sigma} - ik_y^r Y_{r,\sigma})$, with $X_{r,\sigma} = -i\ (a_P\partial r_P/\partial\theta_i - i\sigma a_S\partial r_S/\partial\theta_i)/(r_P a_P - i\sigma r_S a_S)/k^i$, $Y_{r,\sigma} = (r_P + r_S)\ (ia_S - \sigma a_P)\cot\theta_i/(r_P a_P - i\sigma r_S a_S)/k^i$, $b_2 = r_s a_s/r_p/a_p$. By performing the inverse Fourier transform of equation (6), the coordinate representation of the electric field for the reflected light beam in circular polarization basis can be written as

$$\left|E_{\sigma}^{r}\right\rangle = \frac{r_P a_P}{\sqrt{2}}\left(1 + \frac{k^r X_{r,\sigma}x_r}{z_R + iz_r} + \frac{k^r Y_{r,\sigma}y_r}{z_R + iz_r}\right).$$
$$\times\exp\left[-\frac{1}{2}k^r\frac{(x_r)^2 + (y_r)^2}{z_R + iz_r}\right]d_{r,\sigma}\left|e_{r,\sigma}\right\rangle, \tag{7}$$

where $z_R = k^r w_0^2/2$, $d_{r,\sigma} = 1 - i\sigma b_2$, $k^r = k^i$.

The expression of the longitudinal spin splitting for the reflected light beam using the defined spin splitting formula $\Delta_{T,\sigma} = \langle E_{\sigma}^r|x_r|E_{\sigma}^r\rangle / \langle E_{\sigma}^r|E_{\sigma}^r\rangle$ ($z_r = 0$) can be derived as follows:

$$\Delta_{T,\sigma} = \Delta_{\mathrm{GH},\sigma} + \delta_{\sigma}, \tag{8}$$
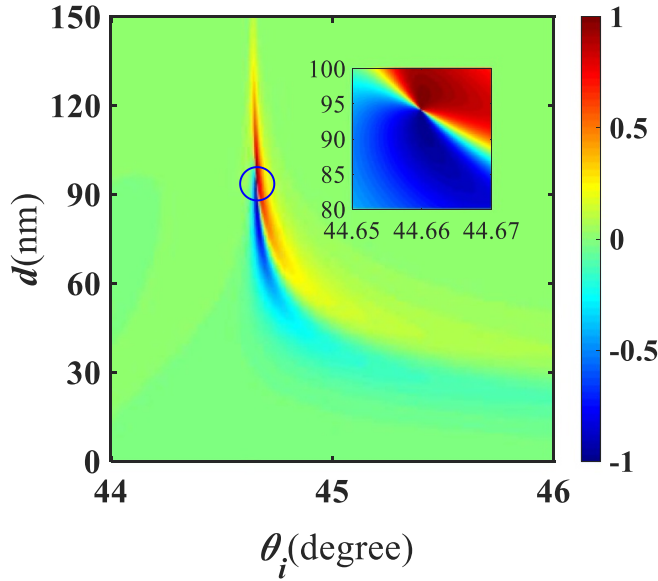
Figure 2. $\partial |r_P| /\partial\theta_i$ as functions of the sodium film thickness d and the incident angle θ_i. The inset picture shows the results near the SPR angle.

with

$$\Delta_{\mathrm{GH},\sigma} = \frac{|a_P|^2\,\mathrm{Im}(r_P{}^*\partial r_P/\partial\theta_i) + |a_S|^2\,\mathrm{Im}(r_S{}^*\partial r_S/\partial\theta_i)}{Mk^i(1+\sigma g)}, \tag{8a}$$

$$\delta_\sigma = \sigma\,\frac{\mathrm{Re}[(a_P a_S{}^* r_S{}^*\partial r_P/\partial\theta_i) - (a_P{}^* a_S r_P{}^*\partial r_S/\partial\theta_i)]}{Mk^i(1+\sigma g)}, \tag{8b}$$

where $M = |r_P|^2|a_P|^2 + |r_S|^2|a_S|^2 + [(|C_y|^2 + |a_P|^2|\partial r_P/\partial\theta_i|^2 + |a_S|^2|\partial r_S/\partial\theta_i|^2)/(k^i w_0)^2]$, $\quad g = 2\,\mathrm{Im}(r_P{}^* r_S a_P{}^* a_S) + 2\,\mathrm{Im}[a_P{}^*\cdot a_S(\partial r_P{}^*/\partial\theta_i)(\partial r_S/\partial\theta_i) + a_P{}^* a_S|C_y|^2]/(k^i w_0)^2/M$, with $C_y = (r_P + r_S)\cot\theta_i$. The g is the asymmetric spin splitting factor.

The relative permittivity of sodium film selected as the SPR excitation metal is expressed as [30]:

$$\varepsilon_2(\omega) = \varepsilon_b - \frac{\omega_p^2}{\omega^2 + i\omega\gamma_p} + \frac{f_1\omega_1^2}{\omega_1^2 - \omega^2 - i\omega\gamma_1}. \tag{9}$$

The fitting parameters of the sodium film are given: $\varepsilon_b = 0.500$, $\omega_p = 5.414$ eV, $\omega_1 = 2.945$ eV, $f_1 = 0.280$, $\gamma_1 = 2.706$ eV and $\gamma_p = 0.010$ eV [30]. Figure 2 shows that the $\partial |r_P| /\partial\theta_i$ as function of the incident angle and the thickness of the sodium film. In the numerical simulations, the parameters were chosen as follows $\varepsilon_1 = 1.446^2$ [33], $\varepsilon_3 = 1$, $\lambda_0 = 1310$ nm. $\partial |r_P| /\partial\theta_i$ is equal to zero at $d = 94$ nm and $\theta_i = 44.66°$ (where the SPR is excited, the angle of incidence corresponding to the SPR excitation is represented by θ_i^{SPRE}).

Interestingly, the value of g corresponding to incident light of the arbitrary state of polarization (SOP) tends to zero when the SPR is excited, as shown in figure 3. This means that the reflected arbitrary polarized light beam can also obtain the LSSS (including two extreme cases: longitudinal
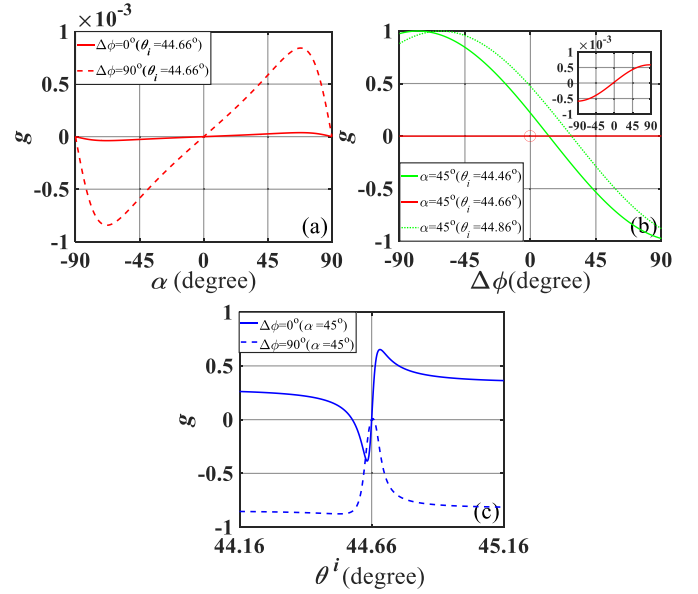
Figure 3. (a) g varying with incident angle θ_i, (b) g varying with the amplitude ratio angle α and (c) g varying with the phase difference $\Delta\phi$, when the SPR is excited. $\lambda_0 = 1310$ nm, $w_0 = 300\lambda_0/\pi = 125\ \mu$m.

spin-dependent splitting disappears completely and only longitudinal spin-independent shift occurs, i.e. $\Delta_{T,\sigma} = \Delta_{\mathrm{GH}}$; longitudinal spin-independent shift disappears completely and only longitudinal spin-dependent splitting occurs, i.e. $\Delta_{T,\sigma} = \delta_\sigma$). Thus, when the SPR is excited, equation (8) can be simplified as

$$\Delta_{T,\sigma} = \Delta_{\mathrm{GH}} + \delta_\sigma, \tag{10}$$

with

$$\Delta_{\mathrm{GH}} = \frac{|a_P|^2\,\mathrm{Im}(r_P{}^*\partial r_P/\partial\theta_i) + |a_S|^2\,\mathrm{Im}(r_S{}^*\partial r_S/\partial\theta_i)}{Mk^i}, \tag{10a}$$

$$\delta_\sigma = \sigma\,\frac{\mathrm{Re}[(a_P a_S{}^* r_S{}^*\partial r_P/\partial\theta_i) - (a_P{}^* a_S r_P{}^*\partial r_S/\partial\theta_i)]}{Mk^i}. \tag{10b}$$

The first term of equation (10) represents the spin-independent shift, which is essentially the Goos–Hänchen (GH) shift [34–37], and the second term of equation (10) is the spin-dependent splitting, which is the focus of the following discussion.

3. Giant longitudinal SHE for elliptically polarized light under SPR

The Stokes parameter S_3 of the non-uniformly polarized reflected light field depends on the spatial coordinates. To reveal the physical mechanism of the LSSS of arbitrarily elliptically polarized light, the average of the reflected light field Stokes parameter S_3 is defined by:

$$\bar{S}_3 = \frac{\langle E^r | S_3(x,y) | E^r \rangle}{\langle E^r | E^r \rangle}. \tag{11}$$

where $|E^r\rangle = [(E_R^r + E_L^r)|e_{r,P}\rangle + i(E_R^r - E_L^r)|e_{r,S}\rangle]/\sqrt{2}$, with E_R^r, E_L^r are the right-handed circularly polarized basis component and the left-handed circularly polarized basis component of the reflected light field expressed by equation (7), respectively. $S_3(x,y) = \langle E_J^r|\hat{\sigma}_2|E_J^r\rangle$, $\hat{\sigma}_2$ is the Pauli operator, $|E_J^r\rangle$ is the Jones space representation of the SOP of reflected light field. $\hat{\sigma}_2$ and $|E_J^r\rangle$ is represented as:

$$\hat{\sigma}_2 = \begin{pmatrix} 0 & -i \\ i & 0 \end{pmatrix}$$

$$|E_J^r\rangle = \begin{pmatrix} r_P a_P \left(1 - i\frac{\partial r_P}{r_P \partial \theta_i}\frac{x_r}{z_R} + i\frac{r_P + r_S}{r_P}\frac{a_S \cot\theta_i}{a_P}\frac{y_r}{z_R}\right) \\ r_S a_S \left(1 - i\frac{\partial r_S}{r_S \partial \theta_i}\frac{x_r}{z_R} - i\frac{r_P + r_S}{r_S}\frac{a_P \cot\theta_i}{a_S}\frac{y_r}{z_R}\right) \end{pmatrix}.$$

According to equation (11), $\bar{S}_3$ can be further calculated as:

$$\bar{S}_3 = \frac{2(|r_P a_P|^2 + |r_S a_S|^2)\,\text{Im}(r_P{}^* a_P{}^* r_S a_S) + B}{|r_P a_P|^2 + |r_S a_S|^2 + A} \quad (12)$$
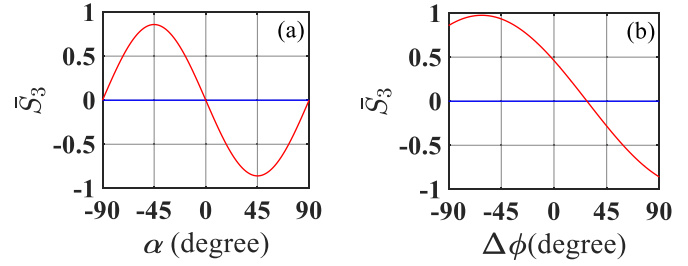
with,

$$A = \frac{1}{(k^i w_0)^2}\left[|r_P a_P|^2\left(\left|\frac{\partial r_P}{r_P \partial \theta_i}\right|^2 + \left|\frac{r_P + r_S}{r_P}\frac{a_S}{a_P}\right|^2\cot^2\theta_i\right)\right.$$
$$\left. + |r_S a_S|^2\left(\left|\frac{\partial r_S}{r_S \partial \theta_i}\right|^2 + \left|\frac{r_P + r_S}{r_S}\frac{a_P}{a_S}\right|^2\cot^2\theta_i\right)\right];$$

$$B = \frac{4}{(k^i w_0)^2}\left\{\text{Re}\left[r_S{}^* a_S{}^* r_P a_P\left(\frac{\partial r_P}{r_P \partial \theta_i} - \frac{\partial r_S{}^*}{r_S{}^* \partial \theta_i}\right)\right]\right.$$
$$\times \left[|r_P a_P|^2\,\text{Im}\left(\frac{\partial r_P}{r_P \partial \theta_i}\right) + |r_S a_S|^2\,\text{Im}\left(\frac{\partial r_S}{r_S \partial \theta_i}\right)\right]$$
$$- \text{Re}\left[r_S{}^* a_S{}^* r_P a_P\left(-\frac{r_P + r_S}{r_P}\frac{a_S}{a_P} - \frac{r_P{}^* + r_S{}^*}{r_S{}^*}\frac{a_P{}^*}{a_S{}^*}\right)\right]\cot^2\theta_i$$
$$\left. \times \left[|r_P a_P|^2\,\text{Im}\left(\frac{r_P + r_S}{r_P}\frac{a_S}{a_P}\right) + |r_S a_S|^2\,\text{Im}\left(\frac{r_P + r_S}{r_S}\frac{a_P}{a_S}\right)\right]\right\}.$$

The $\bar{S}_3$ essentially reflects the average helicity of the reflected light field. The blue solid lines in figures 4(a) and (b) clearly show that the $\bar{S}_3$ is very insensitive to the change of the phase difference and is close to zero when the SPR is excited. However, the $\bar{S}_3$ varies significantly with the phase difference when the SPR is not excited, as shown in the red solid lines in figures 4(a) and (b). Obviously, $\bar{S}_3$ tends to zero, which means symmetric spin splitting occurs. Furthermore, similar to the reflected linearly polarized light beam, the reflected elliptically polarized light beam with arbitrary phase difference can also produce the LSSS when the SPR is excited. To give a clear comparison, figure 5 plots the spatial distribution of the $S_3(x,y)$. It can be seen that there is a close connection between $\bar{S}_3$ and symmetric spin splitting. It is worth emphasizing that the LSSS value of elliptically polarized light beam is so small that it is almost negligible for $\theta_i = 44.86°$, $\alpha = 45°$, $\Delta\phi = 28.25°$ as shown in figure 5(b).

One can see from figures 6(a)–(c) $\text{Re}(r_P)$, $\text{Im}(r_P)$, $\text{Re}(\partial r_S/\partial \theta_i)$ and $\text{Im}(\partial r_S/\partial \theta_i)$ tend to zero, and can be ignored compared to $\text{Re}(\partial r_P/\partial \theta_i)$, $\text{Im}(\partial r_P/\partial \theta_i)$, $\text{Re}(r_S)$ and $\text{Im}(r_S)$,

Figure 4. (a) $\bar{S}_3$ changing with α at the phase difference $\Delta\phi = 90°$, (b) $\bar{S}_3$ changing with $\Delta\phi$ at the amplitude ratio angle $\alpha = 45°$, for different incident angle $\theta_i = 44.66$ (solid blue lines), and $\theta_i = 44.86$ (solid red lines). $\lambda_0 = 1310$ nm, $w_0 = 300\lambda_0/\pi = 125$ μm.
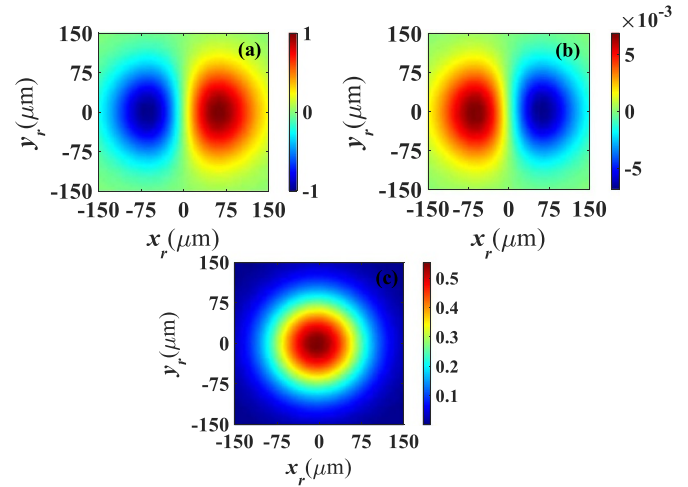
**Figure 5.** Spatial distribution of $\bar{S}_3$ of the reflected elliptical polarized light field. (a) $\theta_i = 44.66°$, $\alpha = -70°$, $\Delta\phi = 90°$; (b) $\theta_i = 44.86°$, $\alpha = 45°$, $\Delta\phi = 28.25°$; (c) $\theta_i = 44.86°$, $\alpha = -70°$, $\Delta\phi = 90°$.

when the incident angle is very close to the θ_i^{SPRE}. At this time, as long as α for the linearly polarized light or elliptically polarized light is not very close to 0° and 90°, Δ_{GH} can be negligible compared to δ_σ. Furthermore, equation (10) can be simplified to

$$\Delta_{T,\sigma} = \sigma\frac{\text{Re}[(a_P a_S{}^* r_S{}^* \partial r_P/\partial \theta_i)]}{Mk^i}. \quad (13)$$

In general, the SHE is the symmetrical splitting of the intensity distribution of the two spin components of the reflected or refracted light, so the total spin splitting represented by equation (13) is an elegant LSSS, which can also be regarded as a longitudinal SHE, similar to the transverse SHE [1, 2]. It is worth noting that another view holds that the SHE is an optical effect in which the beam displacement is proportional to the spin of the incident light [13]. According to this viewpoint, the transverse SHE associated with Imbert–Fedorov shift appears. The longitudinal SHE of the linearly polarized light can be further simplified as $\Delta_{T,\sigma} = \sigma\sin 2\alpha\,\text{Re}(r_S{}^* \partial r_P/\partial \theta_i)/(Mk^i)$, while the longitudinal SHE of the elliptically polarized light for $\Delta\phi = 90°$ can be reduced to $\Delta_{T,\sigma} = \sigma\sin 2\alpha\,\text{Im}(r_S{}^* \partial r_P/\partial \theta_i)/(Mk^i)$.

To illustrate that the longitudinal SHE of elliptically polarized light is stronger than that of linearly polarized light,
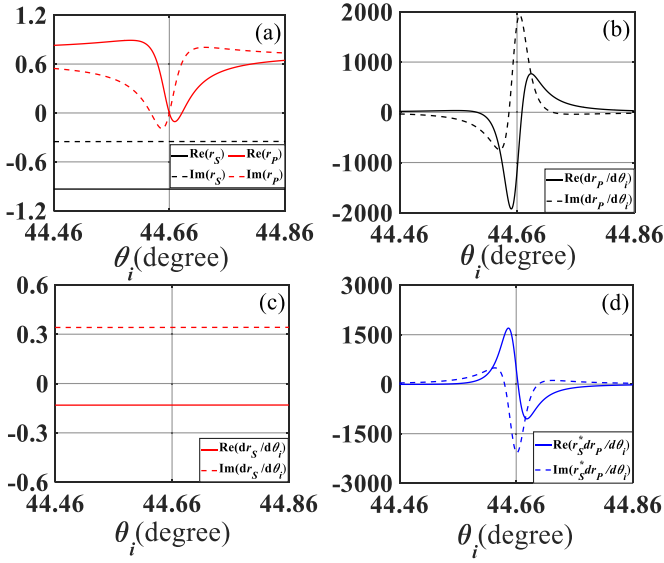
Figure 6. (a) r_P, r_S; (b) $\partial r_P/\partial \theta_i$; (c) $\partial r_S/\partial \theta_i$; (d) $r_S^* \partial r_P/\partial \theta_i$ varying with incident angle θ_i.

$\text{Im}(r_S^* \partial r_P/\partial \theta_i)$ and $\text{Re}(r_S^* \partial r_P/\partial \theta_i)$ as a function of incident angle, are plotted as shown in figure 6(d). It can be clearly shown that $\text{Im}(r_S^* \partial r_P/\partial \theta_i)$ corresponding to the elliptically polarized light with $\Delta \phi = 90°$ is significantly larger than $\text{Re}(r_S^* \partial r_P/\partial \theta_i)$ corresponding to the linearly polarized light when the SPR is excited. For the above reasons, the longitudinal SHE of the elliptically polarized light with $\Delta \phi = 90°$ is significantly larger than that of the linearly polarized light, as shown in figure 7(a). Figure 7(b) further shows that the incident elliptically polarized light can also produce the giant longitudinal SHE. The longitudinal SHE value of the reflected light beam reaches 60.28 μm when the amplitude ratio angle α is equal to 70° and the phase difference $\Delta \phi$ is equal to 90°. The spin splitting direction of the giant longitudinal SHE can be dynamically and flexibly switched by changing the amplitude ratio angle α and the phase difference $\Delta \phi$, which is quite different from previous reports that the linearly polarized light is used to obtain the giant longitudinal SHE [22, 38]. Even incident circularly polarized light can also achieve the giant longitudinal SHE, and this interesting optical effect clearly reveals that achieving giant longitudinal SHE is essentially determined by the mean SOP of the reflected light beam. It is interesting to revisit the longitudinal photonic spin splitting in the incident circular polarization basis. The longitudinal spin splitting of arbitrarily polarized light can be viewed as a superposition of the spin splitting caused by normal and abnormal modes. In order to clearly show the details of the superposition of spin splitting caused by these two modes, we take the longitudinal spin splitting of right-handed circularly polarized light incidence as an example. The Fresnel coefficient matrix under the circular polarization representation is a matrix with cross-Fresnel coefficients as follows:

$$\hat{F}^r = \begin{pmatrix} r_{RR} & r_{RL} \\ r_{LR} & r_{LL} \end{pmatrix}, \tag{14}$$

with $r_{RR} = r_{LL} = \frac{r_P + r_S}{2}$, $r_{RL} = r_{LR} = \frac{r_P - r_S}{2}$.
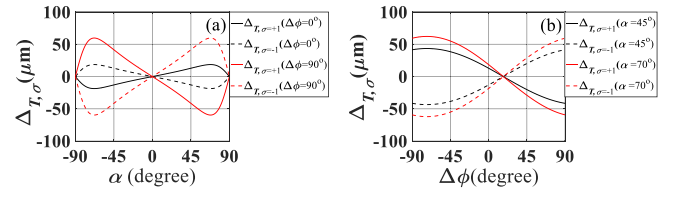
Figure 7. (a) Spin-dependent shifts $\Delta_{T,\sigma}$ for $\Delta \phi = 0°$ and $\Delta \phi = 90°$ changing with α, (b) spin-dependent shifts $\Delta_{T,\sigma}$ changing with $\Delta \phi$ for $\alpha = 45°$ and $\alpha = 70°$, when the SPR is excited, $w_0 = 300\lambda_0/\pi = 125$ μm.
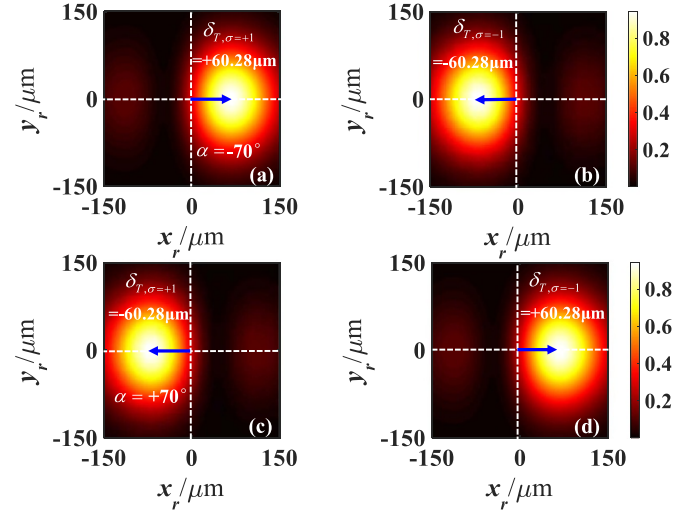
Figure 8. Intensity distributions of two spin components of the reflected beams when an incident elliptically polarized light beam with $\Delta \phi = 90°$ strikes an prism–sodium interface for $\theta_i = 44.66°$. (a) $\sigma = +1$, $\alpha = -70°$, (b) $\sigma = -1$, $\alpha = -70°$; (c) $\sigma = +1$, $\alpha = +70°$, (d) $\sigma = -1$, $\alpha = +70°$.

When SPR is excited, $\partial |r_P|/\partial \theta_i$ is equal to zero, at which point $\text{Re}(r_P)$, $\text{Im}(r_P)$ is very close to zero, and $\text{Re}(\partial r_P/\partial \theta_i)$, $\text{Im}(\partial r_P/\partial \theta_i)$ are much larger than $\text{Re}(r_S)$, $\text{Im}(r_S)$, $\text{Re}(\partial r_S/\partial \theta_i)$, $\text{Im}(\partial r_S/\partial \theta_i)$, as shown in figures 6(a)–(c). The key factors causing longitudinal spin splitting due to the above reasons satisfy the following relationship:

$$\tilde{x}_R = -\tilde{x}_L, \tag{15}$$

with $\tilde{x}_R = \frac{i}{k^i} \frac{\partial r_{RR}}{r_{RR} \partial \theta_i} = \frac{i}{k^i} \frac{\partial r_P}{r_S \partial \theta_i}$, $\tilde{x}_L = \frac{i}{k^i} \frac{\partial r_{LR}}{r_{LR} \partial \theta_i} = -\frac{i}{k^i} \frac{\partial r_P}{r_S \partial \theta_i}$.

The $\tilde{x}_R$ is associated with normal mode and the $\tilde{x}_L$ is associated with abnormal mode. Therefore, the longitudinal SHE of right-handed circularly polarized light is caused by the symmetrical separation of normal mode and abnormal mode. In the case of arbitrarily elliptically polarized light, the superposition of spin splitting produced by normal mode and abnormal mode is more complex, but its essence remains the same.

To provide a clear physical picture, the intensity distributions of two opposite spin components of a reflected light beam when SPR is excited, are shown in figure 8. One can clearly see that an elegant giant longitudinal SHE exists.

4. Conclusions

In summary, the giant longitudinal SHE of the elliptically polarized light beam is achieved by excited of the SPR based sodium at the telecommunication wavelength. The physical mechanism of the LSSS is revealed by analyzing the asymmetric spin splitting factor and the spatially averaged Stokes parameter $\bar{S}_3$. Remarkably, the direction of spin splitting of the giant longitudinal SHE of elliptically polarized light can be dynamically switched by changing the phase difference $\Delta\phi$ and amplitude ratio angle α. We expect that these findings can help researchers to deeply understand the photonic spin–orbit interaction and provide a new approach for designing precision fiber-optic communication devices.

Data availability statement

The data that support the findings of this study are available upon reasonable request from the authors.

Acknowledgments

ORCID iDs

Ze Chen https://orcid.org/0000-0003-2013-1887
Weiming Zhen https://orcid.org/0000-0001-5948-1679
Hu Zhang https://orcid.org/0000-0002-8795-9753
Yang Meng https://orcid.org/0000-0001-6559-5242

References

[1] Bliokh K Y and Bliokh Y P 2006 *Phys. Rev. Lett.* **96** 073903
[2] Hosten O and Kwiat P 2008 *Science* **319** 787
[3] Bliokh K Y, Rodríguez-Fortuño F J, Nori F and Zayats A V 2015 *Nat. Photon.* **9** 796
[4] Zhu T *et al* 2019 *Phys. Rev. Appl.* **11** 034043
[5] He S, Zhou J, Chen S, Shu W, Luo H and Wen S 2020 *Opt. Lett.* **45** 877–80
[6] Xiao T, Yang H, Yang Q, Xu D, Wang R, Chen S and Luo H 2022 *Opt. Lett.* **47** 925–8
[7] Shah M 2021 *J. Appl. Phys.* **55** 105105
[8] Ling X, Xiao W, Chen S, Zhou X, Luo H and Zhou L 2021 *Phys. Rev.* A **103** 033515
[9] Ling X, Guan F, Cai X, Ma S, Xu H-X, He Q, Xiao S and Zhou L 2021 *Laser Photon. Rev.* **15** 2000492
[10] Ling X, Guan F, Zhang Z, Xu H-X, Xiao S and Luo H 2021 *Phys. Rev.* A **104** 053504
[11] Qin Y, Li Y, Feng X, Xiao Y-F, Yang H and Gong Q 2011 *Opt. Express* **19** 9636–45
[12] Chen S, Mi C, Wu W, Zhang W, Shu W, Luo H and Wen S 2018 *New J. Phys.* **20** 103050
[13] Bliokh K Y, Samlan C T, Prajapati C, Puentes G, Viswanathan N K and Nori F 2016 *Optica* **3** 1039–47
[14] Bliokh K Y, Prajapati C, Samlan C T, Viswanathan N K and Nori F 2019 *Opt. Lett.* **44** 4781–4
[15] Qin Y, Li Y, He H and Gong Q 2009 *Opt. Lett.* **34** 2551–3
[16] Luo L, Qiu X, Xie L, Liu X, Li Z, Zhang Z and Du J 2017 *Opt. Express* **25** 21107–14
[17] Zhu W, Zhuo L, Jiang M, Guan H, Yu J, Lu H, Luo Y, Zhang J and Chen Z 2017 *Opt. Lett.* **42** 4869–72
[18] Takayama O, Sukham J, Malureanu R, Lavrinenko A V and Puentes G 2018 *Opt. Lett.* **43** 4602–5
[19] Kim M, Lee D, Kim T H, Yang Y, Park H J and Rho J 2019 *ACS Photonics* **6** 2530–6
[20] Dong P, Cheng J, Da H and Yan X 2020 *New J. Phys.* **22** 113007
[21] Jia G, Zhang R, Huang Z, Ma Q, Wang H and Asgari R 2021 *New J. Phys.* **23** 073010
[22] Zhou X, Xie L, Ling X, Cheng S, Zhang Z, Luo H and Sun H 2019 *Opt. Lett.* **44** 207–10
[23] Yoshikawa N, Tamaya T and Tanaka K 2017 *Science* **356** 736–8
[24] Yao F, Chen C L, Harvey T A and Prum R O 2018 *Nat. Commun.* **9** 3387
[25] Xie H, Li M, Luo S, Li Y, Tan J, Zhou Y, Cao W and Lu P 2018 *Opt. Lett.* **43** 3220–3
[26] Ayuso D, Neufeld O, Ordonez A F, Decleva P, Lerner G, Cohen O, Ivanov M and Smirnova O 2019 *Nat. Photon.* **13** 866
[27] Chen Z, Zhang H, Zhang X, Li H, Yang J, Zhang W, Xi L and Tang X 2020 *Opt. Express* **28** 29529–39
[28] Fang N, Lee H, Sun C and Zhang X 2005 *Science* **308** 534
[29] Boltasseva A and Atwater H A 2011 *Science* **331** 290
[30] Wang Y *et al* 2020 *Nature* **581** 401
[31] Aiello A and Woerdman J P 2009 Theory of angular Goos–Hänchen shift near Brewster incidence (arXiv:0903.3730)
[32] Salasnich L 2012 *Phys. Rev.* A **86** 055801
[33] Palik E D 1985 *Handbook of Optical Constants of Solids* vol I (New York: Academic)
[34] Goos F and Hänchen H 1947 *Ann. Phys.* **1** 333
[35] Aiello A 2012 *New J. Phys.* **14** 013058
[36] Töppel F, Ornigotti M and Aiello A 2013 *New J. Phys.* **15** 113059
[37] Wu F *et al* 2021 *Phys. Rev.* A **104** 023518
[38] Cai L, Zhang S, Zhu W, Wu H, Zheng H, Yu J, Zhong Y and Chen Z 2020 *Opt. Lett.* **45** 6740–3